

Article

# On Tidal Current Velocity Vector Time Series Prediction: A Comparative Study for a French High Tidal Energy Potential Site

Tony El Tawil <sup>1</sup>, Nicolas Guillou <sup>2</sup> , Jean-Frédéric Charpentier <sup>3,\*</sup> and Mohamed Benbouzid <sup>4,5</sup> 

<sup>1</sup> Naval and Energy Engineering Research & Innovation Unit, Segula Technologies, 92000 Nanterre, France; tony.eltawil@segula.fr

<sup>2</sup> Laboratoire de Génie Côtier et Environnement (LGCE), Direction Eau Mer et Fleuves Environnement et Risques, Cerema, 155 rue Pierre Bouguer Technopôle Brest-Iroise, BP 5, 29280 Plouzané, France; nicolas.guillou@cerema.fr

<sup>3</sup> Institut de Recherche de l'École Navale (IRENav, EA 3634), French Naval Academy, 29240 Brest, France

<sup>4</sup> Institut de Recherche Dupuy de Lôme, (UMR CNRS 6027, IRDL), University of Brest, 29238 Brest, France; Mohamed.Benbouzid@univ-brest.fr

<sup>5</sup> Logistics Engineering College, Shanghai Maritime University, Shanghai 201306, China

\* Correspondence: jean-frederic.charpentier@ecole-navale.fr; Tel.: +33-2-98-23-38-69

Received: 13 December 2018; Accepted: 8 February 2019; Published: 13 February 2019



**Abstract:** Estimating the energy potential of tidal stream site is a key feature for tidal energy system deployment. This paper aims to compare two methods of prediction of tidal current velocities. The first one is based on the use of a fully three-dimensional (3D) numerical approach. However, while being accurate, the numerical model is highly time-consuming. The second method is based on a linear approximation of the tidal current, which only requires preliminary knowledge of local current velocities time series during two typical tidal cycles. This second method allows a very quick evaluation of the tidal stream resource during a long time period. The proposed comparison is done in three different locations of a high potential tidal energy site in west of France. It is carried out in terms of current velocity and energy harnessing for several turbines technology options (with and without yaw). The achieved results show that the linear approximation gives satisfactory evaluation of the tidal stream potential and can be a very interesting tool for preliminary site evaluation and first technology options selection. However, the fully 3D numerical model can obviously be very useful in more advanced steps of a project.

**Keywords:** tidal stream energy; Tidal Current Prediction; Computation Method; site evaluation

## 1. Introduction

In a marine energy project first steps, estimating the energy that can be produced by a harnessing system in its lifetime is a key feature for decision makers [1]. For tidal stream turbines, this harnessed energy strongly depends on the chosen installation site and the technology options [1,2]. High tidal current energy potential is located in hot spots, which are very limited in space in the vicinity of headlands and straits [3]. For example, along the coast of France, only a few spots, such as the “Fromveur strait” near Ouessant island in western Brittany or the “Raz Blanchard” in Normandie, are considered to be economically attractive thanks to very high values of tidal current velocities [4]. Several technological options for tidal stream turbines were developed and tested in the marine environment as part of a series of industrial projects [5]. The proposed technologies may thus rely on (i) a yaw system that allows the turbine axis to follow the fluid velocity direction or (ii) a fixed orientation axis that harnesses the kinetic energy of tidal current along a given orientation. In the

second technological option, variations on the direction of the current velocity vectors may significantly influence the amount of energy that can be harnessed [2]. In the tidal stream energy site of the Raz de Sein (western Brittany), a yearly-averaged misalignment of  $32^\circ$  between ebb and flood current peaks was thus found to lead to a reduction of the monthly-extractable energy by 12% [6].

In situ measurements, based on Acoustic Doppler Current Profiler (ADCP), are typically conducted to characterize the spatial and temporal variability of current amplitude and direction within a tidal stream energy site, and assess the power potential for tidal turbines installation [7–9]. However, these observations are restricted to a limited number of locations and periods to time. Refined numerical assessments of the temporal variabilities of the current velocities, during a significant time (more than one year), are thus required to determine the technological options and the optimal locations of turbines, and guarantee successful deployment of these devices in the marine environment. Several methods may be applied to compute the tidal current velocity vector time series in a given site. In this paper, a comparative study of the efficiency of two computational methods is proposed for three typical locations in the Fromveur Strait (western Brittany, Figure 1), a region with strong potential for tidal array development along the coast of France. The first method is based on the use of a three-dimensional (3D) numerical model (TELEMAC, [10]). Whereas this method allows refined computation of the tidal velocity components, it requires important computational resources and is highly time consuming. The second method is based on the preliminary knowledge of the time series of the current velocity in mean spring and neap tidal cycles, only. In this case, a linear approximation based on the French tidal coefficient (defined by French Navy Oceanographic Service) allows determining the current velocity vectors during any tidal cycle. This method is characterized by a very simple computational algorithm that allows determining very quickly the tidal velocity vector time series during a long evaluation period of time. The results given by these two methods are compared in terms of time series of (i) tidal current vector amplitude and direction, and (ii) global energy harnessed by turbines. The comparison is conducted for several locations and several technological options (turbine with and without yaw).

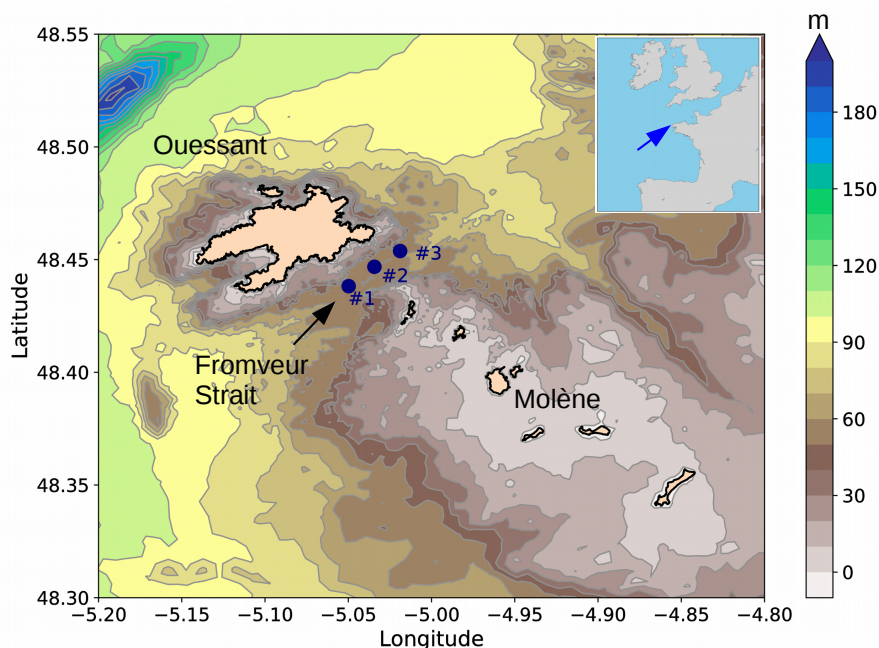


**Figure 1.** Bathymetry of Ouessant-Molène archipelago and the Fromveur Strait with the locations of the three points #1, #2 and #3 retained in the present investigation.

The paper is organized as follows. Sections 2.1 and 2.2 describe the two computational methods investigated and compared. Section 3 presents the tidal stream energy site of the Fromveur Strait

and the three locations retained within this strait to conduct the comparative study. The results are analysed and discussed in Section 4 exhibiting differences in computing tidal current magnitude and associated energy harnessed by a 10 m diameter turbine with yaw and with fixed axis, respectively. Conclusions and perspectives are finally drawn in Section 5.

## 2. Description of the Computational Methods

### 2.1. Numerical Model

The most common way to characterize the hydrodynamic conditions within a tidal stream energy site is based on the implementation of a high-resolution numerical model assessed against in-site measurements. In the present investigation, predictions of tidal currents derived thus from the three-dimensional numerical model TELEMAC 3D [10] have been implemented by Guillou and Chapalain [6] in western Brittany. The model solves the continuity and Reynolds-averaged momentum equations relying on the finite-element method and the implementation of a computational mesh of triangular elements. Further details about this numerical resolution method are available in [10]. The planar computational grid was thus composed of 51,226 nodes duplicated along the vertical direction following an uniform  $\sigma$ -transformation with 15 levels (Figure 2). This transformation enables to have a constant number of computational nodes along the vertical following the variation of the water depth from offshore to nearshore regions. The horizontal grid was composed of unstructured elements that capture, at high-spatial resolution, the complex coastline geometry of tidal strait surrounding by isles and islets, and shoals while sparing computational costs with a reduced number of grid nodes at offshore sea boundaries. A spatial horizontal resolution of less than 50 m was thus reached in the Fromveur strait while it was set to 10 km at offshore sea boundaries.

The numerical model was parameterized and calibrated according to the implementation performed by Guillou and Thiébot [11] and Guillou et al. [12] in western Brittany. The mean water depth derived from (i) the HOMONIM (“Historique, Observation, Modélisation des Niveaux Marins”) database in coastal waters [13] and (ii) the regional database of Loubrieu et al. [14] in offshore areas. Particular attention was furthermore devoted to the parameterization of the bottom roughness that was determined by matching (i) sediment bottom types from the map established by Hamdi et al. [15] with (ii) roughness observations compiled by Soulsby [16]. The horizontal eddy viscosity was parametrised following Smagorinsky [17]. The vertical eddy viscosity was computed with the mixing length model proposed by Quetin [18]. Neglecting the influence of wind-generated surface-gravity waves, surface wind and thermal fronts, the model was driven by major harmonic tidal constituents of the TPX08-atlas database, only [19]. This database covers the area of interest with a spatial resolution of  $1/30^\circ$ . The model performances were finally evaluated against available measurements of tidal current amplitude and direction at two locations, within the Fromveur Strait and in the north of Molène Island. These local evaluations were complemented by a synoptic evaluation of model predictions against numerical estimations provided by the French Navy Oceanographic Service SHOM in mean spring tidal conditions. Further details about the assessment of numerical results are available in [11].

The present investigation relied on the predictions of depth-averaged tidal currents amplitude and direction, achieved during the year 2016, at three locations within the Fromveur Strait (Section 3, Figure 2). This simulation took approximately 88 CPU hours to perform all the model simulations, using 8 cores of a 2048 core system, based on Intel Xeon processors.

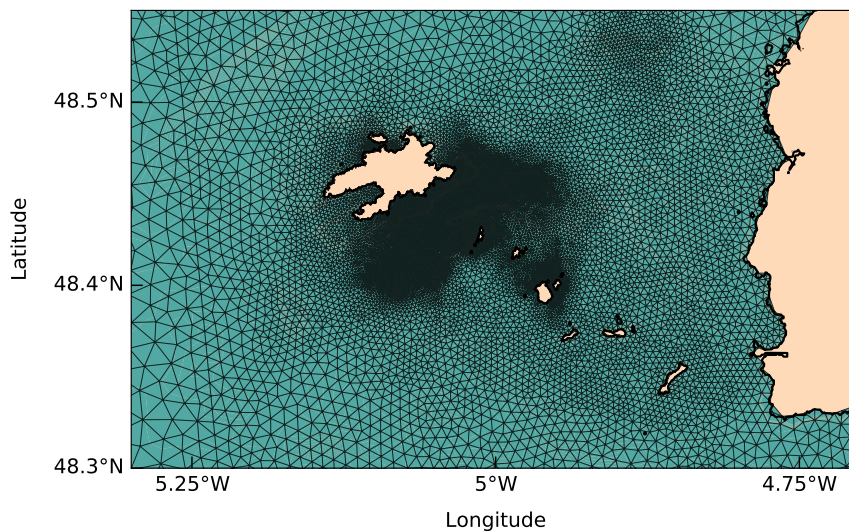


**Figure 2.** Detailed view of the unstructured computational grid of TELEMAC around Ouessant-Molène archipelago.

### 2.2. Linear Approximation

In the context of this study, the variable considered was the velocity vector varying over a tidal cycle. The method proposes a linearization of this vector as a function of the tidal coefficient. The tidal coefficient is a general parameter initially introduced by Laplace to characterize, in a very simple manner, the tidal range along the coast of France and enables rapid predictions of high and low tides [20]. For a given tidal cycle, this parameter is in practice computed, in the harbor of Brest (French western Brittany), as the ratio between (i) the tidal range that results from semi-diurnal harmonic components and (ii) a reference value taken equal to 6.1 m. The tidal coefficient is thus a non-dimensional number that varies between 20 (for exceptional neap conditions) and 120 (for exceptional spring conditions). Furthermore, the tidal coefficient is constant for each tidal cycle, but varies from one cycle to another. In the present investigation, the velocity vector  $\vec{V}$ , over a given tidal period, in a given geographical point, was computed with a simple linear relationship as

$$\overline{\vec{V}(t_i)} = V(t_i) + \frac{c - 45}{95 - 45} (\overline{\vec{V}_{95}(t_i)} - \overline{\vec{V}_{45}(t_i)}) \quad (1)$$

where  $t_i$  is the tidal time of the considered cycle,  $c$  is the tidal coefficient of this cycle,  $\overline{\vec{V}_{45}(t_i)}$  and  $\overline{\vec{V}_{95}(t_i)}$  are the velocity vectors over mean neap and spring tidal cycles for time  $t_i$ , respectively. Mean neap and spring conditions correspond to tidal coefficients of 45 and 95, respectively. For practical reasons, these reference values were derived from predictions of the numerical model (Section 2.1). In this case only 2 tidal periods are needed. However these reference cycles can also be extracted from measurement or external calculation data base as those given by SHOM in France [21]. In fact, each cycle is characterized with a tidal coefficient,  $c$ , and a cycle starting time and ending time. To be able to achieve the calculation, each of the considered cycles is divided in regular time interval ( $t_i$ ) (in the presented case 12 intervals are considered for each cycle). That means that the value of the time interval ( $t_{i+1} - t_i$ ) can vary from one cycle to one other. For a better understanding, Figure 3 presents a graphical representation of the linear approximation calculation of a given value of  $V(t_i)$  (Equation (1)) for a time  $t_i$  and a tidal coefficient  $c$  for aligned velocity vectors. Results issued from this simple method can be calculated in any geographical point as shown in [2], with nearly negligible computational time (nearly instantaneous), will be compared with predictions from the numerical model characterized by more prohibitive CPU resources (Section 4).

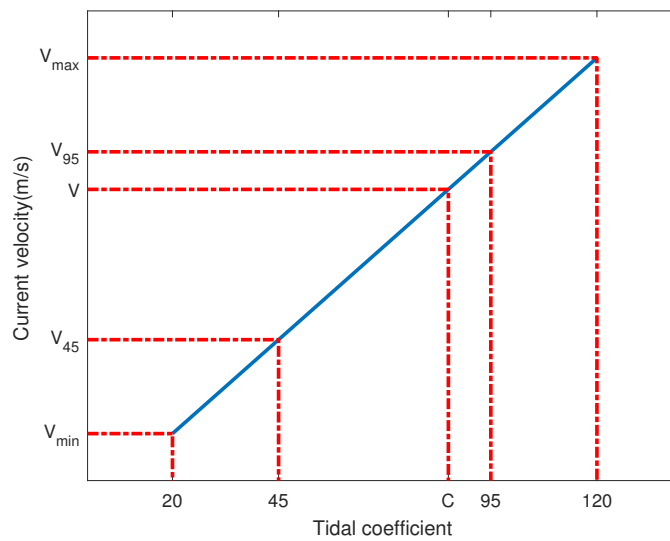


Figure 3. Linear approximation.

### 3. Site Description and Selected Locations

The Fromveur Strait that separates the island of Ouessant from the Molène archipelago through a 2 km wide and 50 m deep strait (Figure 1) is one of the largest tidal stream energy resource along the coast of France with annual peak velocities exceeding  $4 \text{ m s}^{-1}$  [4,21]. Guillou et al. [12] estimated that the available tidal stream power density may reach values over  $20 \text{ kW m}^{-2}$  at 10 m above the seabed in mean spring tidal conditions. The exploitation of the kinetic energy of tidal currents within this environment is thus a very interesting solution to supply a part of clean renewable resources in the electricity grids of Ouessant and Molène whose energetic consumptions rely mainly on fuel power station. Following this roadmap, the company Sabella is experimenting currently, in the Fromveur Strait, a horizontal-axis demonstrator turbine without yaw and pitch system, and with a diameter of 10 m. This device is connected to the electricity grid of the island of Ouessant to meet around 10% of the energy need.

Three points have been selected in the most interesting part (in term of tidal energy potential and turbine operation) of the archipelago, (Fromveur Strait) which has been selected for industrial deployment of the Sabella D10 tidal turbine [5].

The hydrodynamic conditions of the strait are characterized by a strong asymmetry of tidal currents magnitude associated with (i) a northeastern area experiencing flood-dominated flows, and (ii) a southward area experiencing ebb-dominated flows [4,6]. In the 3 chosen sites, the directions of ebb and flood tidal flow are mainly oriented in a common axis. The present investigation focused on three locations defined with respect to this tidal current asymmetry (These 3 points are located in the bathymetry map of Figure 1 and presented in Table 1): location #2 in the central area characterized by equivalent magnitude of flood and ebb peaks (Figure 4), and locations #1 and #3 in the flood and ebb-dominated regions, respectively (Figures 5 and 6). In spring tidal conditions, location #1 exhibited thus peak flood currents of  $3.7 \text{ m s}^{-1}$  against peak ebb currents of  $2.2 \text{ m s}^{-1}$  (Figure 4), this tidal current asymmetry being restricted to less than  $0.2 \text{ m s}^{-1}$  at location #2 (Figure 5).

Table 1. Characteristics of locations #1, #2 and #3 (Figure 1).

Locations	Longitude	Latitude	Mean Water Depths
# 1	5.049° W	48.438° N	58 m
# 2	5.034° W	48.447° N	56 m
# 3	5.019° W	48.454° N	54 m

Using tidal coefficient tables [22], mean neap ( $C = 45$ ) and spring tidal ( $C = 95$ ) periods were identified: the neap tidal period starts at 18h36 (UTC+2) on March 17th and ends at 7h23 (UTC+2) on 18 March, the spring tidal period starts at 12h03 (UTC+2) on 11 January and ends at 0h22 (UTC+2) on 12 January. Figure 7 displays the current velocity vectors predicted by TELEMAC (Section 2.1) for these two tidal cycles (each vector corresponds to a period of approximately one hour) at the three locations #1, #2 and #3.

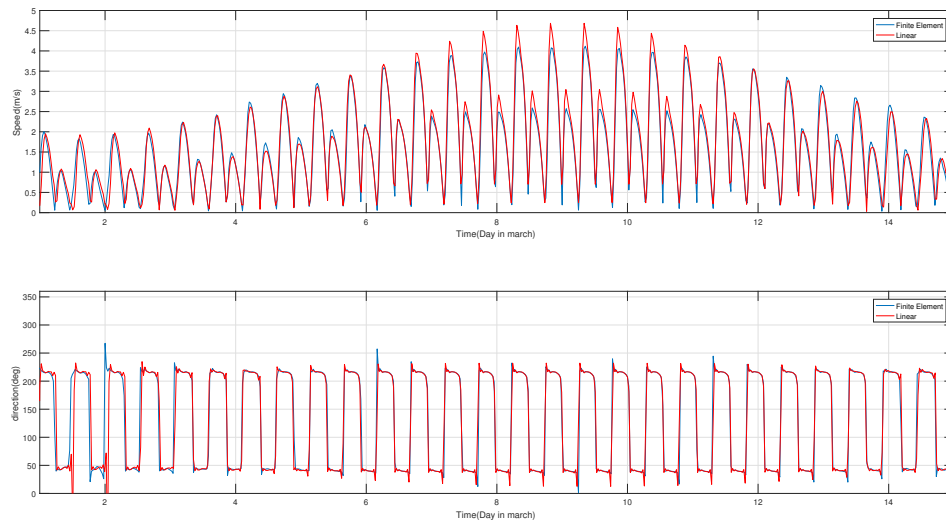


**Figure 4.** Time series of the predicted depth-averaged amplitude and direction (anticlockwise convention from the east) of the current at point #1 in neap-spring tidal cycle.

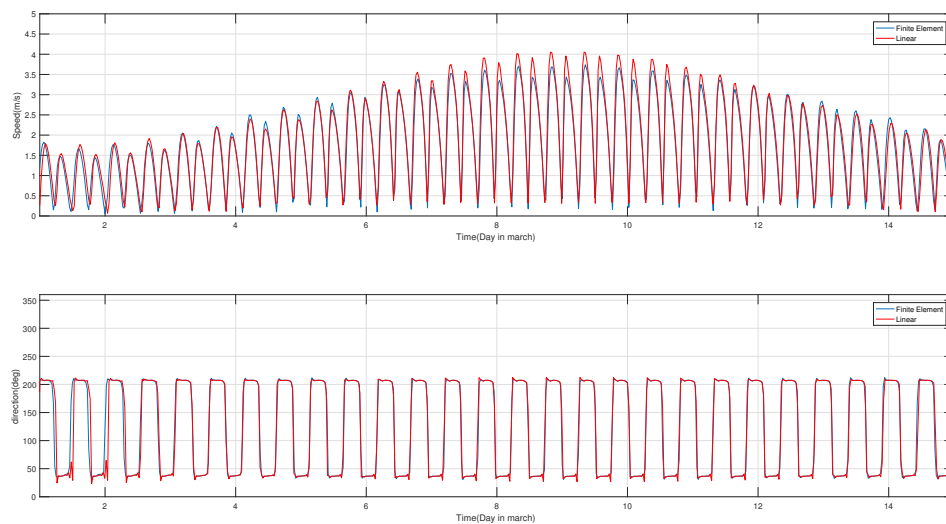


**Figure 5.** Time series of the predicted depth-averaged amplitude and direction (anticlockwise convention from the east) of the current at point #2 in neap-spring tidal cycle.

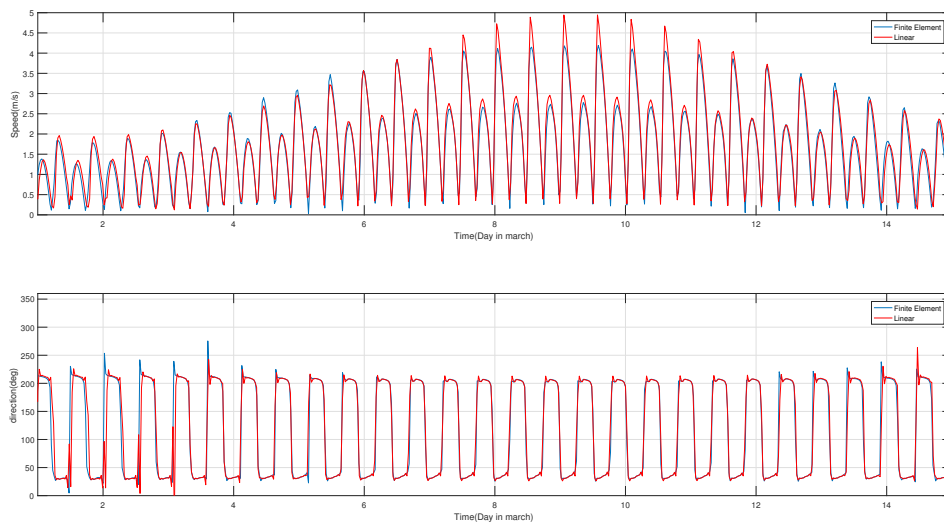


**Figure 6.** Time series of the predicted depth-averaged amplitude and direction (anticlockwise convention from the east) of the current at point #3 in neap-spring tidal cycle.

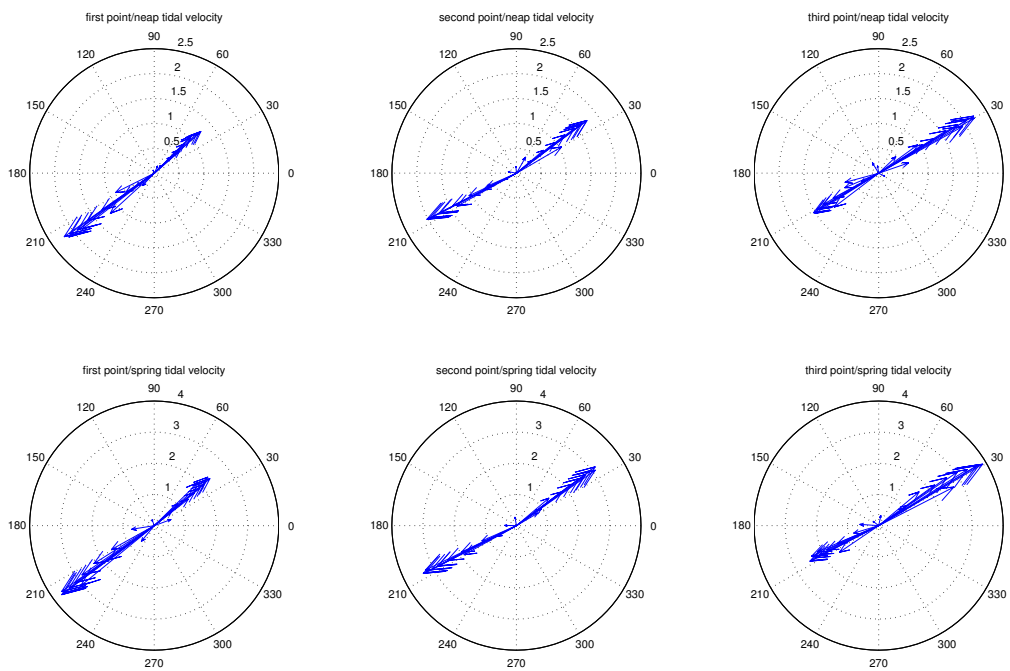


**Figure 7.** Variations of mean neap and spring tidal velocity vectors at the three considered positions.

#### 4. Discussions about the Results

The study evaluated the accuracy of the linear approximation method (Section 2.2) by comparing associated results against predictions from a traditional refined computational method based on numerical modelling of tidal currents in the area of interest, more expensive in time and computing power (Section 2.1). The attention was successively dedicated to the evaluation of tidal currents and tidal stream power and energy.

#### 4.1. Current Time Series Prediction Comparison

Time series of the predicted depth-averaged tidal current amplitude and direction are computed in neap-spring conditions by the two methods at locations #1, #2 and #3 (Figures 4–6). It can be seen that the two methods provide quasi-similar results during this period of time. For a given tidal cycle with a coefficient  $c$ , the relative difference between these two methods was evaluated by the parameter  $e_c$  that assesses the computation of peak tidal currents

$$e_c = \frac{\max(V_{mod,c}) - \max(V_{lin,c})}{\max(V_{mod,c})} \quad \text{for } c = 20 \dots 120 \quad (2)$$

where  $\max(V_{mod,c})$  and  $\max(V_{lin,c})$  are the peak tidal current amplitudes (during a tidal cycle with a coefficient  $c$ ) resulting from the numerical model and the linear approximation methods, respectively. The resulting variation of the relative difference with respect to the tidal coefficient is displayed for the year 2016 in Figure 8. The relative difference followed similar trends at the three locations considered. The difference between the two methods tended thus to reduce when the tidal coefficient value was close to the two references tidal cycle coefficients used in the linear approximation method ( $c = 45$  and  $c = 95$ ). However, this relative difference reached more than 15% for exceptional spring conditions ( $c > 110$ ) and was more important for the two locations characterized by an asymmetry in current amplitude (locations #1 and #3). Indeed, the linear approximation method overestimated the peak values of the velocity for the highest tidal coefficients. These results exhibited the limits of the approximation method for predictions of strong tidal currents. Nevertheless, as the hydrodynamic forces exerted in the systems are approximately proportional to the square of the velocity, this difference in the peak value estimation can lead to a conservative oversizing of structures if only a linear approximation is used.

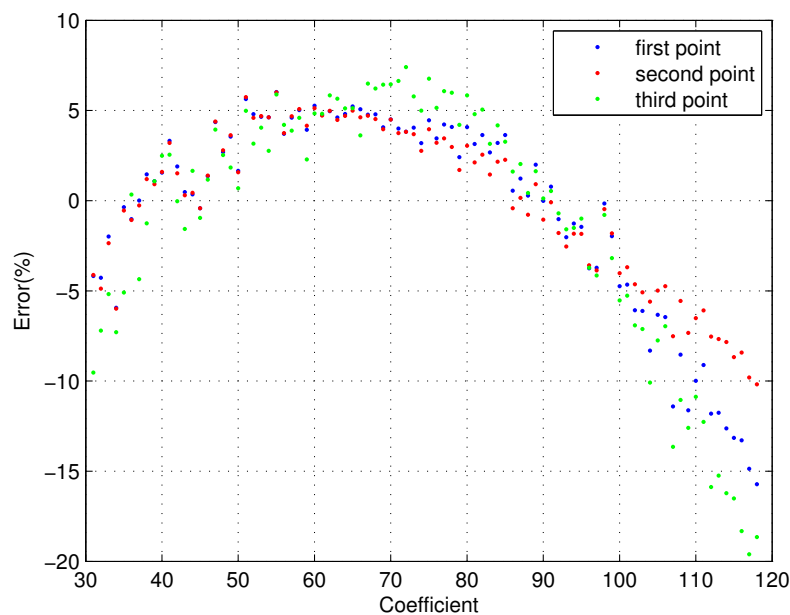


**Figure 8.** Variation of the relative difference  $e_c$  with respect to the tidal coefficient  $c$  during the year 2016 at the three locations #1, #2 and #3.

#### 4.2. Energy Harnessing Comparison with Yawed and Fixed Axis Turbine

After a calculation of the tidal currents during a representative period, the evaluation of the resulting kinetic power and energy harnessed by a system was possible. The kinetic power extracted by a 10 m diameter tidal turbine was considered. Table 2 presents the characteristics of this 10 m diameter tidal turbine [23]. It was first assumed that the extracted power was following the power

vs. velocity curve given in Figure 9. In this configuration, the harnessed power was proportional to the cube of the component of the current along the axis of the system between a cut-in tidal current velocity and a rated tidal current velocity. This part of the curve corresponds to an optimal power extraction (MPPT strategy). For a velocity above the rated value, the power was limited to the rated power in order to limit the energy chain oversizing and the power fluctuations. This power strategy can be implemented using overspeed or underspeed control strategy if a fixed pitch turbine is used or using a variable pitch system if a variable pitch turbine is used [24,25]. Two technological options were then considered. The first one relied on a yaw system that allowed the turbine axis to perfectly follow the current direction at any time. The second technological option considered a fixed axis system. The power was furthermore assumed to be extracted in similar manner in the two-axis direction devices [2]. For yaw systems, the current direction was not integrated in power computation, the energy extracted varying as the amplitude of tidal current at any time (following the power curve in Figure 9). For fixed axis systems, the power was a function (following in similar manner the curve of Figure 9) of the projected speed on the axis of the system [1]. In the latter case, the choice of the direction of the system is obviously critical for an optimal extraction of the energy. In this configuration, the fast calculation, proposed by the linear approximation method, exhibited great interests. Indeed, considering the computation time (a few seconds) necessary to evaluate the variations of the power over one year for a given point, a calculation of the possible 180 positions for a fixed system may be evaluated in a few minutes as explained in El Tawil et al. [2], and the optimal direction may be chosen with an accuracy of 1°.

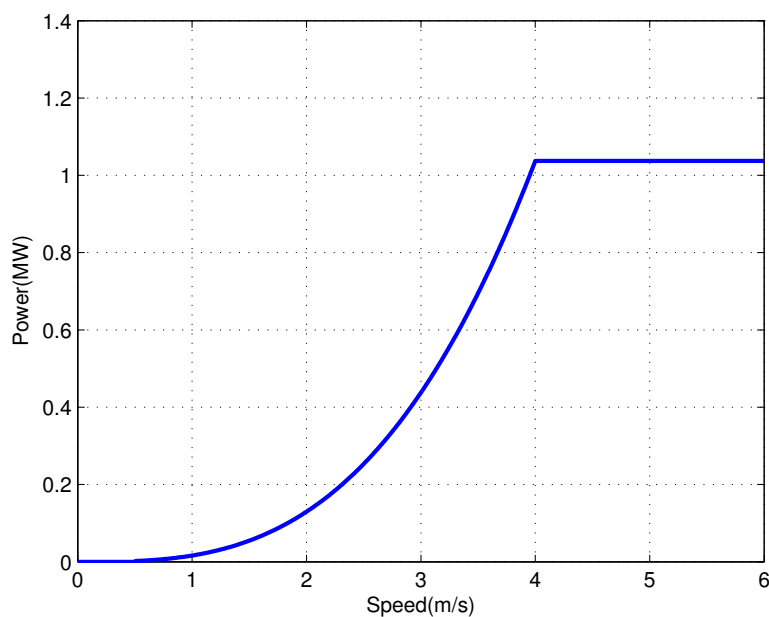


Figure 9. 10m-diameter turbine power production.

Table 2. Characteristics of the 10m-diameter tidal turbine.

Turbine diameter	10 m
Turbine power coefficient	0.4
Cut-in speed	0.5 m/s
Nominal speed	4 m/s
Nominal power	1 MW

Using these characteristics and this axis direction choice method, calculations of the power production of a turbine located on the three positions #1, #2 and #3 were performed for both multidirectional (with yaw) and bidirectional (fixed axis) turbines (Figures 10–12). Table 3 presents a comparison of the harnessed energy calculated during one year between the full 3D Finite Element and the linear approximation methods. In this table, “yawed” and “fixed axis” columns refer to the two different studied turbine technologies. The “difference” columns refer to the relative variation of harnessed energy between fixed axis turbines and yawed ones. For all the cases, reduced differences were obtained in the time series of the predicted power between the two methods. Differences were mainly noticed in predicted power magnitude for strong current velocities in high tidal coefficients. Considering the global results in annual harnessed energy, the two methods allow correct estimation of the extracted power for all the cases with only a few percent differences. The calculated annual difference of harnessed energy related to a yawed or a fixed axis technological choice was also very similar for the two methods. In the three locations retained, the difference of harnessed energy was thus very small. In fact the current velocity vectors, which are not orientated in a common axis corresponded mainly to low amplitude current (during the tide inversion) leading to small power values.

**Table 3.** Estimation of extracted energy at locations #1, #2 and #3 with the detailed and linear approximation methods, for yawed and fixed axis devices, during the year 2016 (results are expressed in MWh).

	Detailed Method			Linear Approximation Method		
	Yawed	Fixed Axis	Difference (%)	Yawed	Fixed Axis	Difference (%)
#1	1193	1190	0.25	1213.6	1204	0.79
#2	1275	1262	0.99	1296.9	1285	0.89
#3	1283	1278	0.37	1281.3	1275	0.44

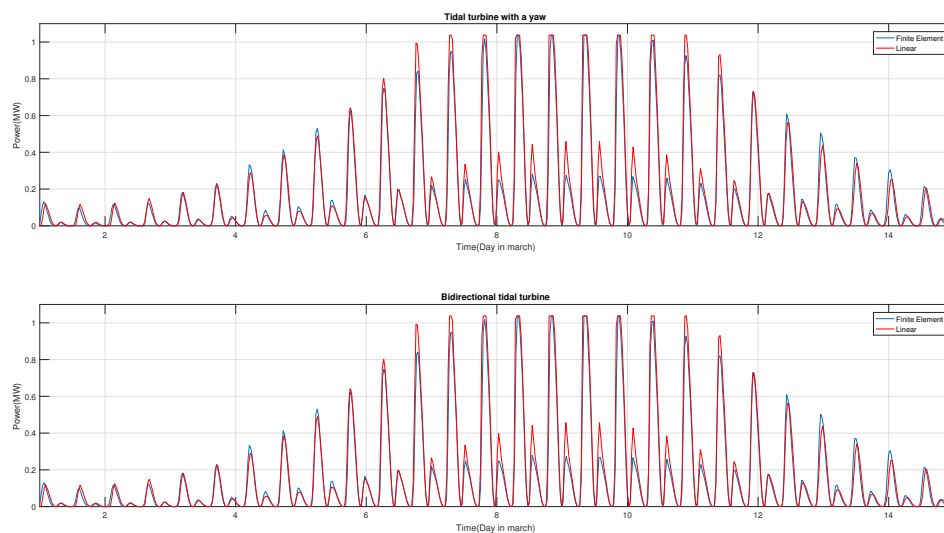


**Figure 10.** Time series of the predicted power production for yawed and fixed-axis turbines at point #1.

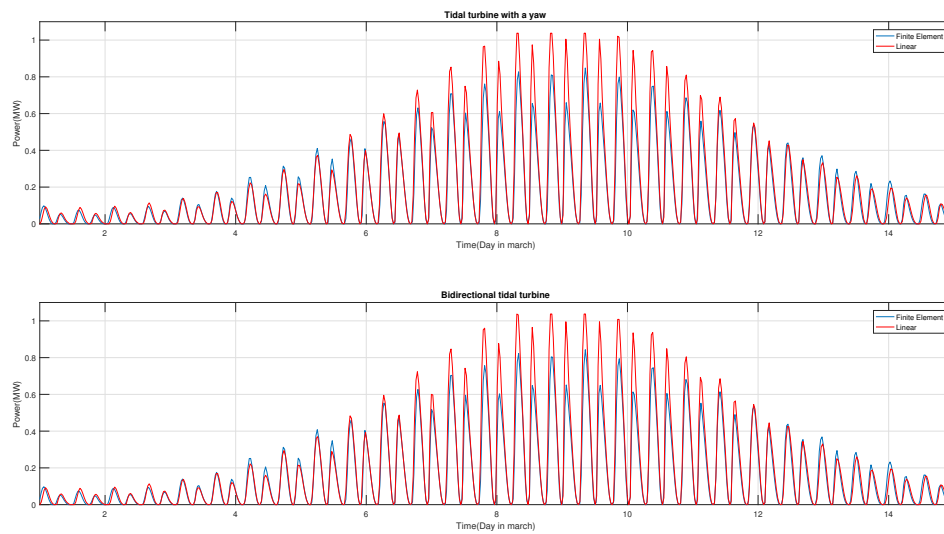


Figure 11. Time series of the predicted power production for yawed and fixed-axis turbines at point #2.

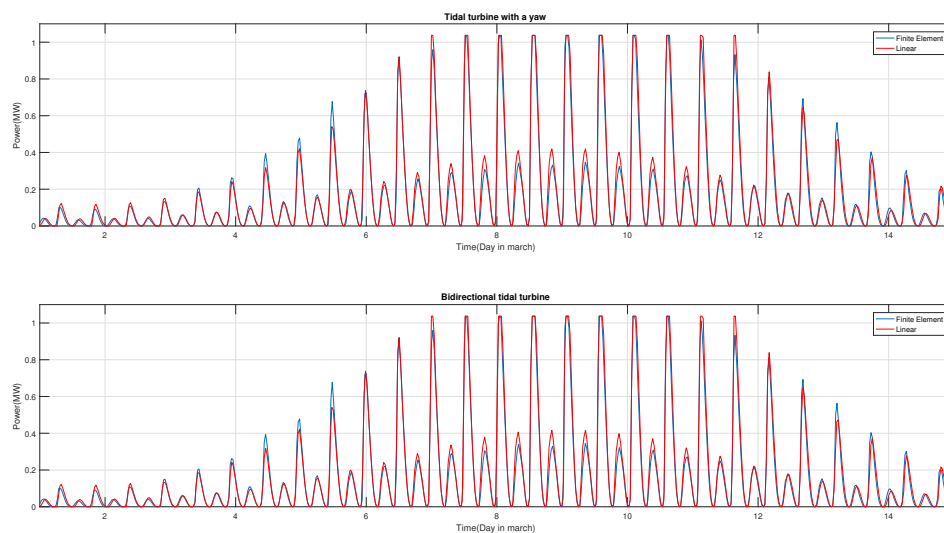


Figure 12. Time series of the predicted power production for yawed and fixed-axis turbines at point #3.

## 5. Conclusions

Two methods have been compared to predict the tidal current velocity vector time series in a French high tidal energy potential site. The first method is based on the direct use of a full 3D finite-element method in a large area and is very precise but highly time-consuming. The second method needs only the knowledge of the current velocity vector for two typical tidal cycles and allows predicting the tidal current evolution at any time by a linear interpolation. This second method is very fast and quick and easy to implement. These two methods have been compared for three locations of a high tidal current energy potential site located in French Brittany. Comparison has been proceeded in terms of current velocity amplitude and direction and in terms of harnessed power and energy considering two 10 m-diameter realistic turbines with two technological options that can significantly influence the harnessed power (yaw system and fixed-axis system). Obtained results show that the two methods give quite similar results for tidal current vector evolution, power and energy. The most significant differences are only related to extreme tidal cycles, where the second method can overestimate the current velocities and the power for the peak values of the tidal current. It can be

conclude that the second method can be a very interesting tool for tidal turbine farm set up in the first steps of a tidal turbine farm project. It allows a very fast estimation of the tidal energy potential in a large area for a significant period of time and can allow decision makers to make preliminary choices of turbines locations and technological options. However, very precise estimation of current velocity in the chosen site is obviously necessary in more advanced steps of a tidal turbine farm project to estimate very precisely the loads on the structures and to adapt technological choices, control strategies and control laws. These more precise predictions can be done by the use of 3D finite element numerical models (as the one presented in Section 2.1) combined with in situ measurement during a significant time period.

**Author Contributions:** Conceptualization, Methodology, Software, Validation, T.E.T. and N.G.; Formal Analysis T.E.T., J.-F.C., N.G. and M.B.; Draft Preparation, Writing, Review, and Editing, T.E.T., J.-F.C., N.G. and M.B.

**Funding:** This research received no external funding.

**Acknowledgments:** Numerical simulations were conducted on HPC facilities DATARMOR of “Pôle de Calcul Intensif pour la Mer” (PCIM) (<http://www.ifremer.fr/pcim>). The present paper is a contribution to the research program DIADEME (“Design et InterActions des Dispositifs d’extraction d’Énergie Marine avec l’Environnement”) of the Laboratory of Coastal Engineering and Environment (Cerema, <http://www.cerema.fr>). This work was also supported by Brest Métropole.

**Conflicts of Interest:** The authors declare no conflict of interest.

## References

- Maslov, N.; Charpentier, J.F.; Claramunt, C. A modelling approach for a cost-based evaluation of the energy produced by a marine energy farm. *Int. J. Mar. Energy* **2015**, *9*, 1–19. [[CrossRef](#)]
- El Tawil, T.; Charpentier, J.F.; Benbouzid, M. Tidal energy site characterization for marine turbine optimal installation: Case of the Ouessant Island in France. *Int. J. Mar. Energy* **2017**, *18*, 57–64. [[CrossRef](#)]
- Neill, S.; Hashemi, M.; Lewis, M. Tidal energy leasing and tidal phasing. *Renew. Energy* **2016**, *85*, 580–587. [[CrossRef](#)]
- Guillou, N.; Neill, S.P.; Robins, P.E. Characterising the tidal stream power resource around France using a high-resolution harmonic database. *Renew. Energy* **2018**, *123*, 706–718. [[CrossRef](#)]
- Zhou, Z.; Benbouzid, M.; Charpentier, J.F.; Sculler, F.; Tang, T. Developments in large marine current turbine technologies—A review. *Renew. Sustain. Energy Rev.* **2017**, *71*, 852–858. [[CrossRef](#)]
- Guillou, N.; Chapalain, G. Tidal Turbines’ Layout in a Stream with Asymmetry and Misalignment. *Energies* **2017**, *10*, 1892. [[CrossRef](#)]
- Epler, J.; Polagye, B.; Thomson, J. Shipboard Acoustic Doppler Current Profiler Surveys to Assess Tidal Current Resources. In Proceedings of the IEEE OCEANS 2010, Sydney, Australia, 24–27 May 2010.
- Fairley, I.; Evans, P.; Wooldridge, C.; Willis, M.; Masters, I. Evaluation of tidal stream resource in a potential array via direct measurements. *Renew. Energy* **2013**, *57*, 70–78. [[CrossRef](#)]
- Carpmand, N.; Thomas, K. Tidal resource characterization in the Folda Fjord, Norway. *Int. J. Mar. Energy* **2016**, *13*, 27–44. [[CrossRef](#)]
- Hervouet, J.M. *Hydrodynamics of Free Surface Flows: Modelling with the Finite Element Method*; John Wiley & Sons: Hoboken, NJ, USA, 2007.
- Guillou, N.; Thiébot, J. The impact of seabed rock roughness on tidal stream power extraction. *Energy* **2016**, *112*, 762–773. [[CrossRef](#)]
- Guillou, N.; Chapalain, G.; Neill, S.P. The influence of waves on the tidal kinetic energy resource at a tidal stream energy site. *Appl. Energy* **2016**, *180*, 402–415. [[CrossRef](#)]
- SHOM. MNT Bathymétrie de la Façade Atlantique (Projet HOMONIM). Available online: <http://diffusion.shom.fr/produits/bathymetrie/mnt-facade-atl-homonim.html> (accessed on 1 September 2017).
- Loubrieu, B.; Bourillet, J.; Moussat, E. *Bathy-Morphologique Régionale du Golfe de Gascogne et de la Manche, Modèle Numérique*; Technical Report; IFREMER: Issy-les-Moulineaux, France, 2008.
- Hamdi, A.; Vasquez, M.; Populus, J. *Cartographie des Habitats Physiques Eunis-Côtes de France*; Technical Report DYNECO/AG/10-26/JP; IFREMER: Issy-les-Moulineaux, France, 2010.

16. Soulsby, R.L. The bottom boundary layer of shelf seas. In *Elsevier Oceanography Series*; Elsevier: Amsterdam, The Netherlands, 1983; Volume 35, pp. 189–266.
17. Smagorinsky, J. General circulation experiments with the primitive equations. I: The basic experiments. *Mon. Weather Rev.* **1963**, *91*, 99–164. [[CrossRef](#)]
18. Quetin, B. Modèles mathématiques de calcul des écoulements induits par le vent. In Proceedings of the 17th Congress of the International Association of Hydraulic Research, Baden-Baden, Germany, 15–19 August 1977.
19. Egbert, G.D.; Bennett, A.F.; Foreman, M.G. TOPEX/POSEIDON tides estimated using a global inverse model. *J. Geophys. Res. Oceans* **1994**, *99*, 24821–24852. [[CrossRef](#)]
20. Simon, B. *La marée La marée Océanique Côtière*; Institut Océanographique: Paris, France, 2007; p. 435.
21. SHOM. *Service Hydrographique et Océanographique de la Marine (2016). Courants de Marée—Mer d'Iroise de L'île Vierge à la Pointe de Penmarc'h*; Technical report 560-UJA; SHOM: Brest, France, 2016.
22. SHOM. Available online: <http://maree.info/82/calendrier> (accessed on 5 September 2018).
23. Ajiwibowo, H.; Lodiwa, K.S.; Pratama, M.B.; Wujanto, A. Field measurement and numerical modeling of tidal current in Larantuka Strait for renewable energy utilization. *Int. J. Geomate* **2017**, *13*, 124–131. [[CrossRef](#)]
24. Zhou, Z.; Scuiller, F.; Charpentier, J.F.; Benbouzid, M.E.H.; Tang, T. Power control of a nonpitchable PMSG-based marine current turbine at overrated current speed with flux-weakening strategy. *IEEE J. Ocean. Eng.* **2015**, *40*, 536–545. [[CrossRef](#)]
25. Arnold, M.; Biskup, F.; Cheng, P.W. Load reduction potential of variable speed control approaches for fixed pitch tidal current turbines. *Int. J. Mar. Energy* **2016**, *15*, 175–190. [[CrossRef](#)]



© 2019 by the authors. Licensee MDPI, Basel, Switzerland. This article is an open access article distributed under the terms and conditions of the Creative Commons Attribution (CC BY) license (<http://creativecommons.org/licenses/by/4.0/>).